Multispectral, multiazimuth, and multioffset coherence attribute applications

Satinder Chopra[1] and Kurt J. Marfurt[2]

Abstract

The coherence attribute computation is typically carried out as a poststack application on 3D prestack migrated seismic data volumes. However, since its inception, interpreters have applied coherence to band-pass-filtered data, azimuthally limited stacks, and offset-limited stacks to enhance discontinuities seen at specific frequencies, azimuths, and offsets. The limitation of this approach is the multiplicity of coherence volumes. Of the various coherence algorithms that have evolved over the past 25 years, the energy ratio coherence computation stands apart from the others, being more sensitive to the seismic waveform changes rather than changes in their amplitude. The energy ratio algorithm is based on the crosscorrelation of five or more adjacent traces to form a symmetric covariance matrix that can then be decomposed into eigenvalues and eigenvectors. The first eigenvector represents a vertically variable, laterally consistent pattern that best represents the data in the analysis window. The first eigenvalue represents the energy of the data represented by this pattern. Coherence is then defined as the ratio of the energy represented by the first eigenvalue to the sum of the energy of the original data. An early generalization of this algorithm was to compute the sum of two covariance matrices, one from the original data and the other from the 90° phase rotated data, thereby eliminating artifacts about low-amplitude zero crossings. More recently, this concept has been further generalized by computing a sum of covariance matrices of traces represented by multiple spectral components, by their azimuthally limited stacks, and by their offset-limited stacks. These more recently developed algorithms capture many of the benefits of discontinuities seen at specific frequencies, azimuths, and offsets, but they present the interpreter with a single volume. We compare the results of multispectral, multiazimuth, and multioffset coherence volumes with the traditional coherence computation, and we find that these newer coherence computation procedures produce superior results.

Introduction

Coherence is a discontinuity detection attribute, which is applied to stacked migrated seismic data volumes to facilitate the interpretation of geologic structural or stratigraphic discontinuities. In general, coherence is applied to data stacked after migration, and it is available in most workstation interpretation software packages. Various implementations of coherence algorithms have evolved over the past 25 years including crosscorrelation-based (Bahorich and Farmer, 1995), semblance-based (Marfurt et al., 1998), variance-based (Pepper and Bejarano, 2005), Sobel filter-based (Luo et al., 1996, 2003), eigenstructure-based (Gersztenkorn and Marfurt, 1999), and gradient structure tensor-based (Bakker, 2003) algorithms. The algorithms most commonly available on workstation software packages are the semblance and some form of eigenstructure decomposition of covariance matrices. We restrict our analysis to the application of the energy ratio algorithm (Chopra and Marfurt, 2008), which is a variation of the eigenstructure approach. We discussed in detail the applications of coherence attribute to seismic data in Chopra and Marfurt (2007, 2018a, 2018b).

The interpretation of stratigraphic features on seismic data is dependent on their bandwidth. In general, seismic data that have a higher bandwidth also provide greater lateral resolution, resulting in sharper coherence images. However, because of tuning, some frequencies may be more sensitive to a given lateral stratigraphic discontinuity than others. Likewise, a given seismic wavelet may show two different horizons to be "aligned" across a fault (e.g., Libak et al., 2017), whereas a wavelet at a different frequency may be misaligned. For these reasons, sometimes interpreters run spectral decomposition (Partyka et al., 1999) or compute spectral voice components prior to computing coherence (Chopra and Marfurt, 2016). In general,

[1]TGS, Calgary, Alberta, Canada. E-mail: satinder.chopra@tgs.com (corresponding author).
[2]The University of Oklahoma, Norman, Oklahoma, USA. E-mail: kmarfurt@ou.edu.

Manuscript received by the Editor 15 May 2018; revised manuscript received 30 October 2018; published ahead of production 05 December 2018; published online 15 March 2019. This paper appears in *Interpretation*, Vol. 7, No. 2 (May 2019); p. SC21–SC32, 13 FIGS.
http://dx.doi.org/10.1190/INT-2018-0090.1.

higher frequency spectral magnitudes or voice components highlight lateral variation in thinner beds, whereas lower frequency magnitude or voice components highlight lateral changes in thicker beds. Another tool at their disposal is the red-green-blue blending of three frequency components, which allows interpreters to corender the information content at different scales. Although useful, this color display tool has a limitation

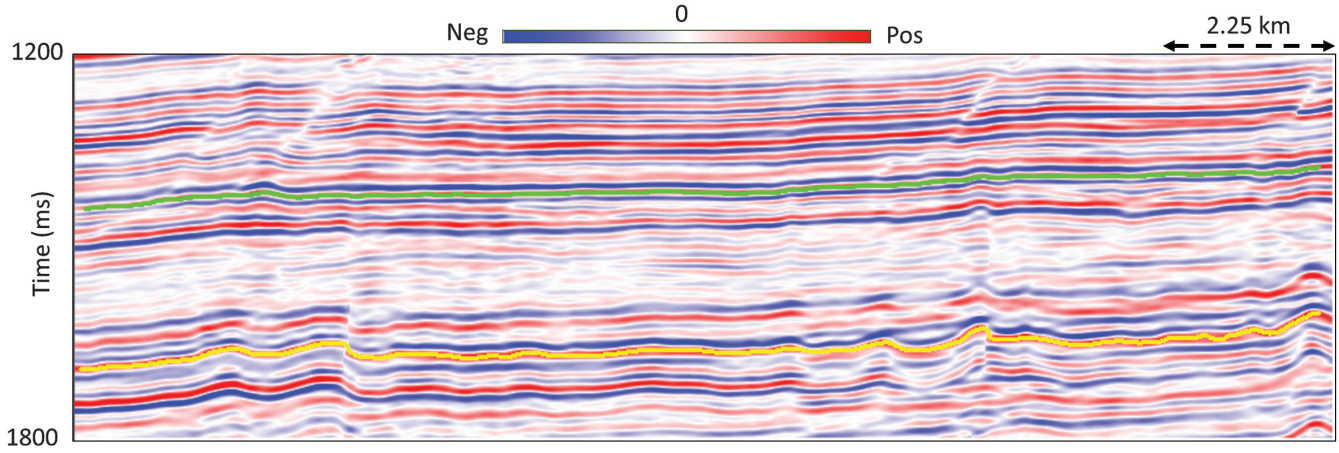

Figure 1. A vertical slice through a 3D seismic amplitude volume from the Montney-Dawson area of northeast British Columbia. The data had been put through one pass of structure-oriented filtering, and the interpreted horizons are shown in green and yellow (data courtesy of TGS, Calgary).

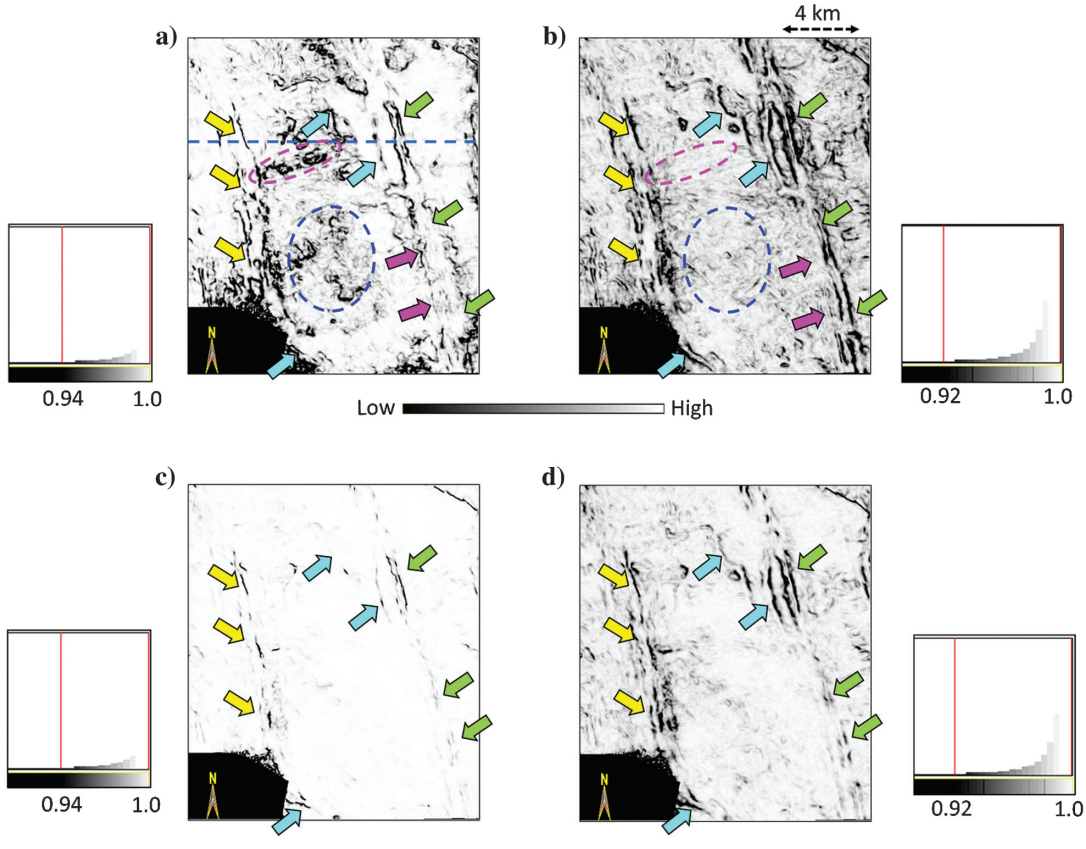

Figure 2. Stratal slices 36 ms above the yellow horizon shown in Figure 1 through (a) coherence volume generated on the full-offset stack and (b) multispectral coherence volume generated by using 12 selected voice component (20, 25, 30, 35, 40, 45, 50, 55, 60, 65, 70, and 75 Hz) volumes. Similar stratal slices generated along the yellow horizon though the (c) full-offset stack and (d) multispectral coherence volume. The seismic data are from the Montney-Dawson area in British Columbia, Canada. Notice the overall better definition of faults (indicated by the yellow, cyan, and green arrows) and the paleochannels (indicated with the magenta arrows) on the multispectral coherence volume shown in Figure 3b and 3c (data courtesy of TGS, Calgary).

in that it can show only three components at a time (Henderson et al., 2008).

Obviously, if a given spectral component highlights a feature of interest, one can delineate edges in such volumes using coherence. The same argument applies to azimuthally limited, offset-limited, or angle-limited partial stacks of the migrated data. Because of amplitude variation with offset effects, lithologic "edges" may be stronger on coherence computed on the far-offset stack. Similarly, faults and other discontinuities will be better illuminated by a perpendicular rather than a parallel azimuthally limited partial stack (Chopra and Marfurt, 2007). Unfortunately, there are two major drawbacks to this "component analysis" workflow. First, each spectral component or partial stack has a lower signal-to-noise content than the broadband or full-stack data volume. Second, the interpreter is now faced with interpreting multiple coherence images, one for each component, which (because of their lower signal-to-noise ratio) can be tedious and very time consuming.

Marfurt (2017) describes a way to construct a multispectral covariance matrix by summing the covariance matrices for all the input spectral components each of which is oriented along the structural dip using analytic voice components. The energy ratio coherence computed using this approach is referred to as multispectral coherence. Qi et al. (2017) extend this concept to azimuthally limited and offset-limited partial stacks, resulting in "multiazimuth" and "multioffset" coherence.

Recall that the seismic response across offsets is sensitive to changes in lithology, porosity, and fluid content. Therefore, we expect that the attribute images generated from offset-limited volumes will show some sensitivity to these changes. In fact, the stratigraphic effects have the maximum influence on the near-offset range, and the lithology and fluid have the greatest effect on the longer offsets. When the seismic amplitudes are stacked over all offsets, we obtain some average of all these responses.

Although the presence of hydrocarbons can cause changes in seismic response with offset or incident

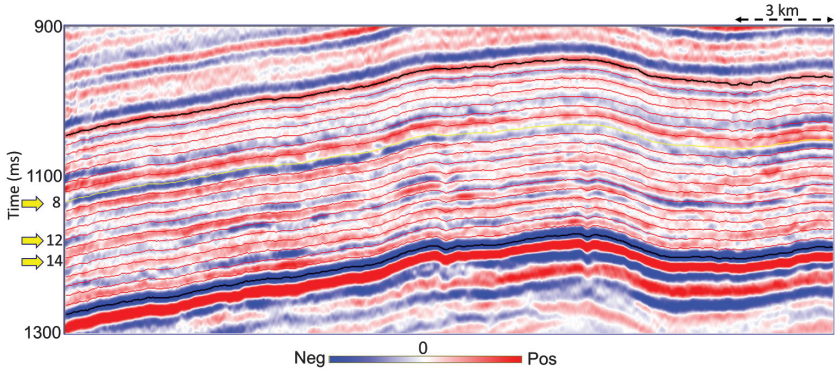

Figure 4. A segment of a seismic section from the Montney-Dawson area in northeast British Columbia in Canada. Stratal slices have been generated between two horizons in black and are shown in red. Displays along stratal slices numbered 8, 12, and 14 are shown in Figure 5 (data courtesy of TGS, Calgary).

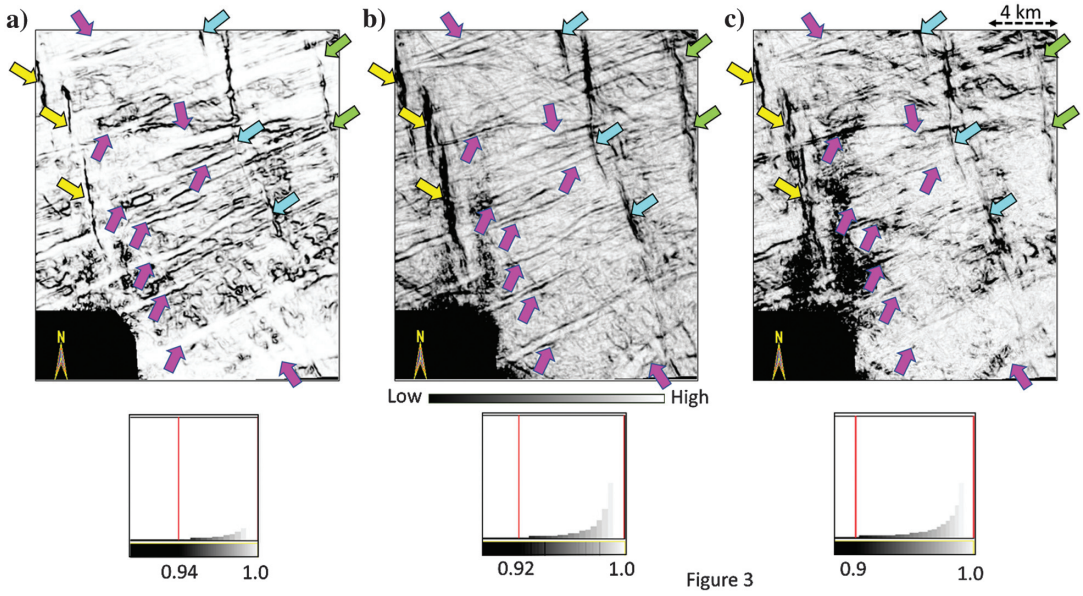

Figure 3

Figure 3. Stratal slices 38 ms above a horizon at approximately 1400 ms through (a) coherence volume generated on the full-offset stack, (b) multispectral coherence volume generated by using 12 selected voice component (20, 25, 30, 35, 40, 45, 50, 55, 60, 65, 70, and 75 Hz) volumes, and (c) multispectral coherence volume generated by using six selected voice component (50, 55, 60, 65, 70, and 75 Hz) volumes. The seismic data are from the Montney-Dawson area in British Columbia, Canada. Notice the overall better definition of faults (indicated with the yellow, cyan, and green arrows) and the paleochannels (indicated with the magenta arrows) on the multispectral coherence volume shown in (b) (data courtesy of TGS, Calgary).

angle, aligned vertical faults and fractures cause azimuthal variations in the seismic amplitude, phase, and velocity (Grimm et al., 1999; Lynn, 2018a, 2018b). The routine production processing typically stacks all azimuths; thus, it obliterates the azimuthal variation of moveout and amplitude.

In this paper, we examine the interpretational value of these recent developments. First, does coherence computed from band-limited, offset-limited, or azimuth-limited stacked seismic volumes contain information that is in some way greater than that of the broadband or stacked image? Second, do multispectral,

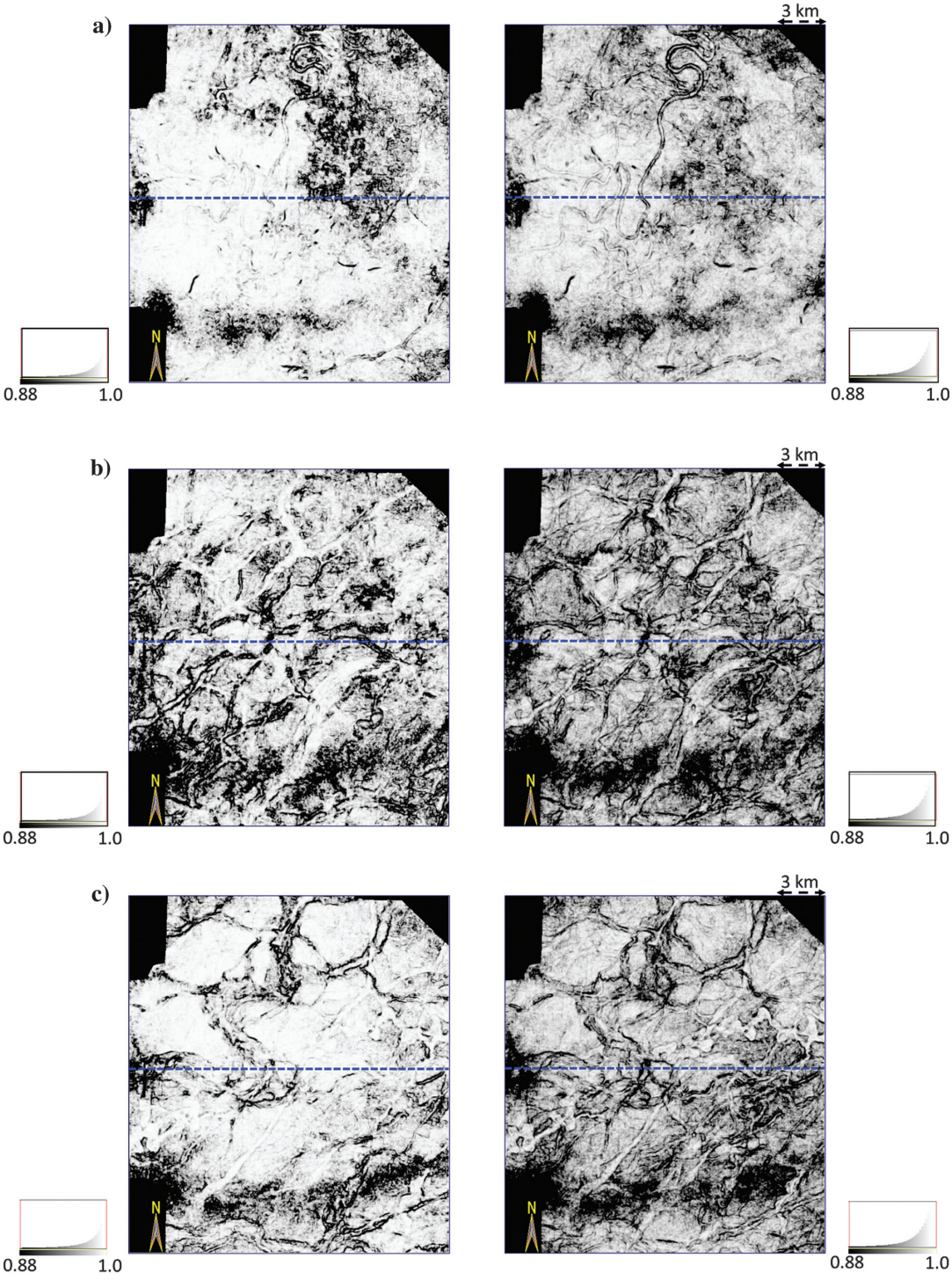

Figure 5. Displays from the conventional (left) and multispectral (right) coherence volumes shown for stratal slices (a) 8, (b) 12, and (c) 14 marked in Figure 4. In all these displays, the definition of the channel displays is better defined; thus, it is more easily interpretable on slices through the multispectral coherence volumes (data courtesy of TGS, Calgary).

multiazimuth, or multioffset images capture any of this lost information?

Multispectral coherence

The energy ratio coherence algorithm has been described in detail, along with applications, by Chopra and Marfurt (2007, 2018a). We briefly mention some of the salient details that would lead us to the applications we describe in this paper.

In the energy ratio algorithm, the covariance matrix is computed from the analytic trace composed of the seismic data $\mathbf{d}$ and its Hilbert transform $\mathbf{d^H}$ along the structural dip, to prevent "structural leakage," corresponding to zero crossings (Chopra and Marfurt, 2007). We define the covariance matrix $\mathbf{C}$ for M traces within a $\pm K$ sample window:

$$C_{mn} = \sum_{k=-K}^{K} [d(t_k, x_m, y_m) d(t_k, x_n, y_n) + d^H(t_k, x_m, y_m) d^H(t_k, x_n, y_n)], \quad (1)$$

where t_k is the time of a structurally interpolated sample at a distance (x_m, y_m) about the analysis point at $(x = 0, y = 0, t = 0)$. The C_{mn} component of the covariance matrix is the crosscorrelation of trace m with trace n over $2K + 1$ samples. The value of M typically ranges from 5 (for higher resolution in good data) to 13 (for lower resolution in noisier data). The value of K ranges from two for good-quality data (and to avoid mixing stratigraphy) to no more than $K = T_{\min}/(2\Delta t)$, where $T_{\min}$ is the shortest usable period and Δt is the sample interval.

Most of the covariance matrices we encounter in attribute analysis are symmetric and are decomposed as

$$\mathbf{C}\mathbf{v}^j = \lambda_j \mathbf{v}^{kj}, \quad (2)$$

where $\mathbf{C}$ is an M-by-M square covariance matrix, λ_j is the jth of M eigenvalues, and $\mathbf{v}^j$ is the corresponding eigenvector. Because the matrix is symmetric, the eigenvalues are all nonnegative. The energy ratio coherence computation is given as

$$C_{\text{Energy ratio}} = \frac{\sum_{k=-K}^{+K} \sum_{m=1}^{M} \{[d_{PC}(t_k, x_m, y_m)]^2 + [d^H_{PC}(t_k, x_m, y_m)]^2\}}{\sum_{k=-K}^{+K} \sum_{m=1}^{M} \{[d(t_k, x_m, y_m)]^2 + [d^H(t_k, x_m, y_m)]^2\}}. \quad (3)$$

In the above mathematical expression, the numerator can be interpreted as the energy of the weighted principal component filtered analytic traces, and the denominator can be interpreted as the sum of the energy of the analytic traces or total energy. In simple notation, the energy ratio coherence may be given as

$$C_{\text{Energy ratio}} = \frac{E_{\text{coh}}}{E_{\text{tot}}}. \quad (4)$$

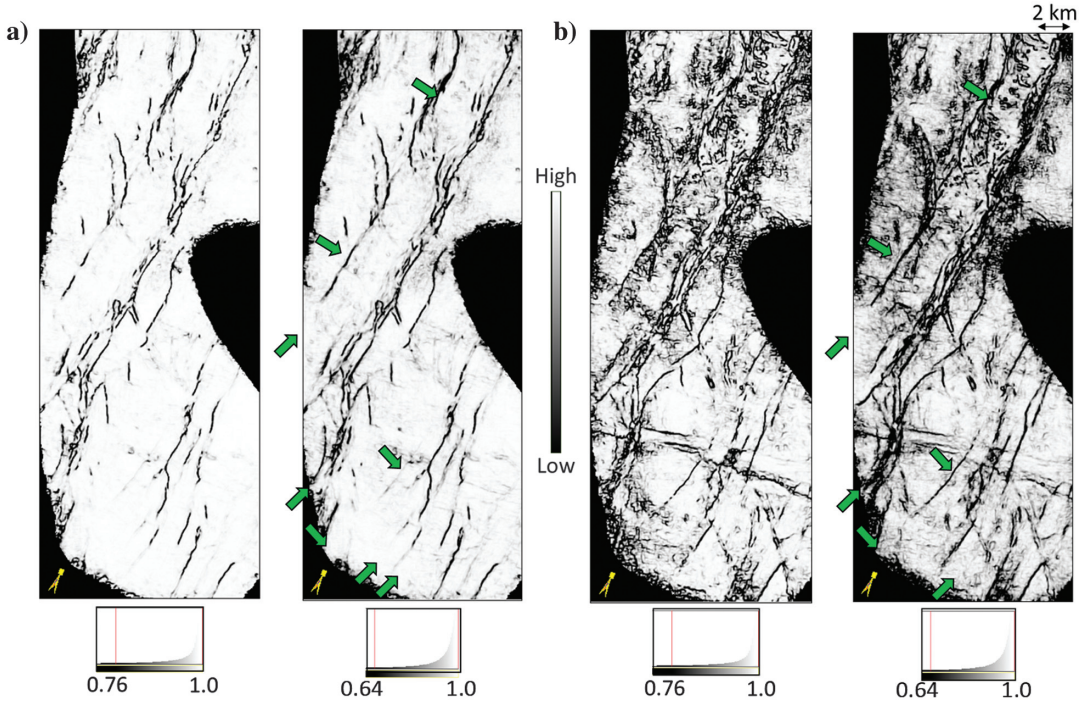

Figure 6. Stratal slices from conventional (left) and multispectral (right) coherence volumes along (a) a horizon picked on the seismic volume at approximately 1200 ms and (b) 68 ms below the horizon in (a). Notice the lineaments on multispectral coherence displays are more focused and continuous resulting in overall more interpretable displays (data courtesy of TGS, Calgary).

Dewett and Hensa (2015) first show the application of multispectral coherence using amplitude and phase information from different frequency bands of the input seismic data. Thereafter, Marfurt (2017) constructs a multispectral covariance matrix oriented along the structural dip using the analytic voice components (equation 1) and, therefore, twice as many sample vectors (i.e., spectral voices and their Hilbert transforms):

$$C_{mn} = \sum_{l=1}^{L} \sum_{k=-K}^{K} [u(t_k, f_l, x_m, y_m)u(t_k, f_l, x_n, y_n) + u^H(t_k, f_l, x_m, y_m)u^H(t_k, f_l, x_n, y_n)]. \quad (5)$$

The corresponding energy ratio coherence computed using this equation is then referred to as *multispectral coherence*.

Multiazimuth coherence

Similar to the multispectral coherence procedure, Qi et al. (2017) generate energy ratio coherence by summing R covariance matrices $\mathbf{C}(\varphi_r)$ computed from each of the R azimuthally limited data volumes:

$$\mathbf{C}_{\text{multi}-\varphi} = \sum_{r=i}^{R} \mathbf{C}(\varphi_r). \quad (6)$$

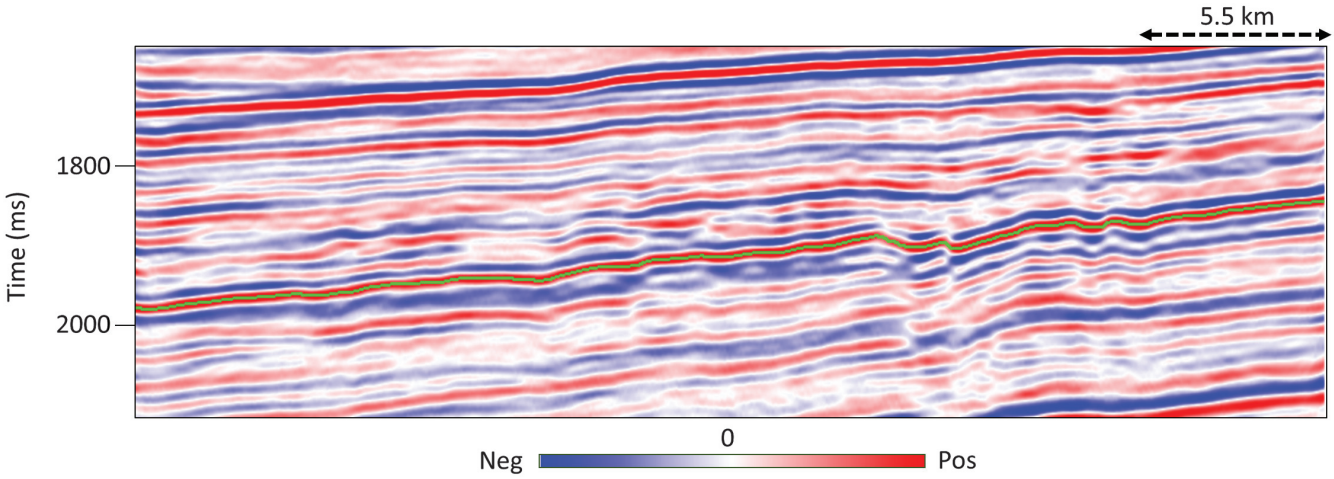

Figure 7. Segment of an inline seismic section from the STACK trend in Oklahoma. Inlines run north–south on the seismic survey as indicated in Figures 8–11 (data courtesy of TGS, Houston).

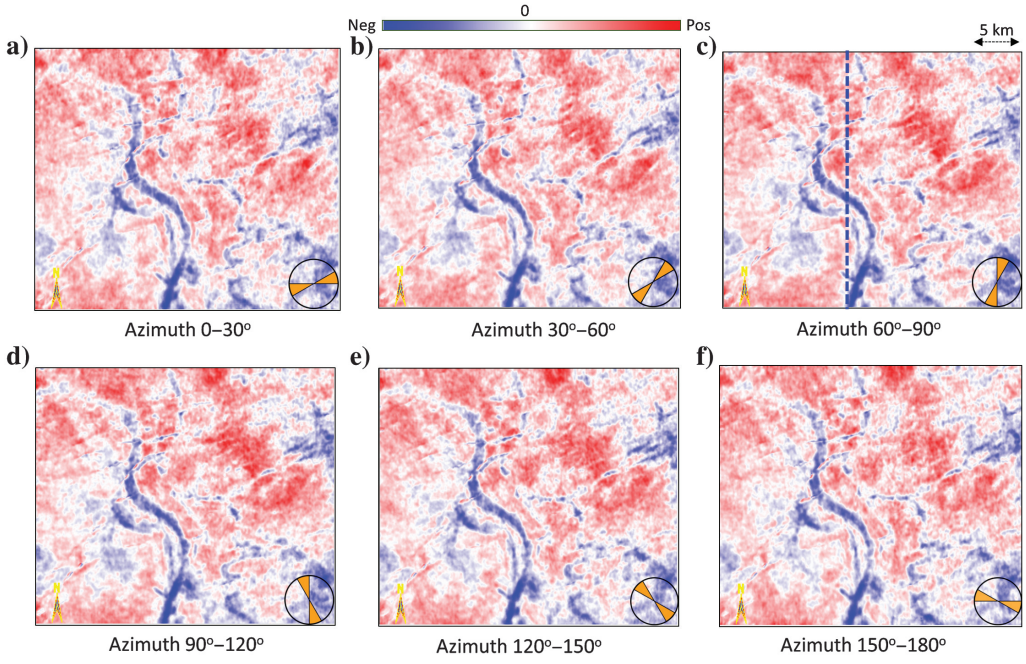

Figure 8. Stratal slices 12 ms above a horizon at approximately 1950 ms from six azimuthally limited partial stack seismic amplitude volumes. The seismic data are from the STACK trend in Oklahoma (data courtesy of TGS, Houston).

The covariance matrix obtained by summation has the same size as the original single-azimuth covariance matrix, but it now has R times as many sample vectors. The "multiazimuth coherence" is computed from $\mathbf{C}_{\text{multi-}\varphi}$ using equations 2 and 3.

Multioffset/multiangle coherence

Multioffset coherence is computed in an analogous manner to multiazimuth coherence. Instead of the azimuthally sectored input volumes, one could use the different offset-limited or angle-limited volumes as the input.

Why the two operations are different

Simple analysis will show that computing R M-by-M covariance matrices and then summing the results is computationally more expensive than summing the R components and computing a single M-by-M covariance matrix. However, because the covariance matrix consists of nonlinear auto- and crosscorrelations, these two operations are not equivalent. Let us use a multiazimuth example as an illustration. Because our velocities are never perfect, the full azimuth stack may be blurred, reducing the coherence anomaly of a small north–south-trending fault. In contrast, the east–west azimuthally limited stack will illuminate this fault well. The covariance matrix then captures the discontinuity through crosscorrelation. Other azimuths may exhibit this discontinuity somewhat less and may be possibly shifted vertically or laterally. Stacking the covariance matrix combines the discontinuities, some constructively, some destructively. Those that persist across multiple azimuths persist. Finally, in our implementation, the magnitude of the individual covariance matrices is proportional to the energy of the components at that spectral, azimuthal, or offset component, thereby weighting the discontinuity by a level of confidence.

Applications

The applications of the three forms of coherence computation discussed above as applied to different data volumes are discussed below.

Multispectral coherence

Figure 1 shows a segment of a section from a 3D seismic data volume from the Montney-Dawson area of northeast British Columbia, Canada. Two horizons have been picked on the seismic data and are used for generation of the stratal slices shown in Figure 2. This data volume was first used to generate the conventional poststack coherence volume. Because the bandwidth of the seismic data was 10–80 Hz, the voice components from 20 to 75 Hz were generated at increments of 5 Hz. These voice components were then used to generate the multispectral coherence. A comparison of the stra-

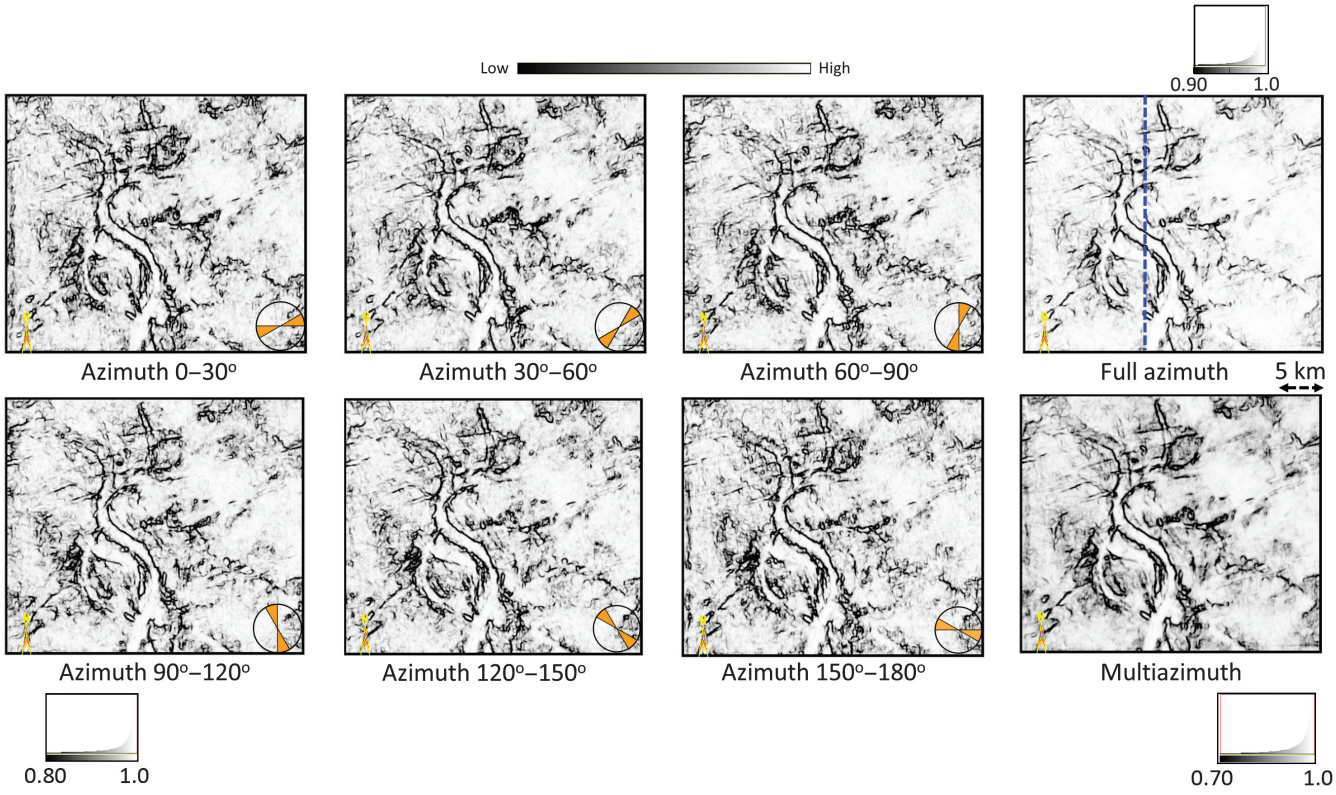

Figure 9. Stratal slices 12 ms above a horizon at approximately 1950 ms through coherence volumes computed from the six azimuthally limited partial stack amplitude volumes shown in Figure 5, from the full stack volume, and using a multiazimuth coherence algorithm. The definitions of the faults as well as the channels are seen much better on the multiazimuth coherence display. The seismic data are from the STACK trend in Oklahoma (data courtesy of TGS, Houston).

tal slices 36 ms above the yellow horizon (shown in Figure 1) from the conventional coherence and the multispectral coherence volumes is depicted in Figure 2a and 2b. The definition of the faults marked with the yellow and green arrows are well-defined on the multispectral coherence display. Similarly, the lineaments indicated with the blue arrows are not seen on the conventional coherence display but appear on the multispectral display. Some of the features seen on the conventional coherence display marked by the magenta arrows or enclosed within the magenta and blue ellipses, disappear on the multispectral coherence. Similarly, the divergence of the fault lineaments indicated by the magenta and green arrows on conventional coherence is not noticed on the multispectral coherence display. We recommend the use of the multispectral and conventional energy ratio coherence so that all the lineament detail can be interpreted on such displays.

Another comparison between the stratal slices generated along the yellow horizon from the same two coherence volumes is shown in Figure 2c and 2d. In this case, because the stratal slice is along a prominent horizon, the trace-to-trace similarity is high; hence, the display shows mostly high coherence values. But even so, the faint lineaments on conventional coherence display (the yellow, blue, and green arrows) are defined clearly on the multispectral coherence display.

Typically, the vertical and spatial resolution increase as the voice component frequency increases. It may therefore be expected that coherence generated from voice components at higher frequencies would show higher spatial resolution. To explore this in the present case, in addition to generating multispectral coherence from voice components ranging from 20 to 75 Hz at 5 Hz increments, another multispectral coherence volume was generated by using frequencies from 50 to 75 Hz at 5 Hz increments. Figure 3 compares the results of these two computations with the conventional "broadband" coherence volume. Notice that the stratal slice from multispectral coherence volume using 12 voice component frequencies shows the best display in that the definitions of the almost-vertical faults (the yellow, blue, and green arrows) stand out the best. Similarly, the paleochannels going almost east–west (the magenta arrows) stand out clearly on this display. The multispectral coherence display in Figure 3c misses out on the definition of some of the feature lineaments that are seen clearly in Figure 3b.

Figure 4 shows a segment of a seismic section from the Montney-Dawson area of northeast British Columbia in Canada. Twenty stratal slices have been generated between two prominent horizons picked on the seismic data and displayed in black. The yellow arrows indicate stratal slices 8, 12, and 14 displayed in Figure 5a–5c through the conventional coherence volume (left column) and multispectral coherence volume (right column). Notice the much better definition of the channel features seen on the multispectral coherence displays.

Figure 6 shows a similar comparison between horizon slices from the conventional coherence (left column) and multispectral coherence (right column). The horizon slices in Figure 6a are generated along a horizon picked on the seismic volume at approximately 1200 ms, whereas those in Figure 6b are generated 68 ms deeper. Again, the lineaments are more focused, continuous and are thus more interpretable on the multispectral coherence slices in Figure 6b.

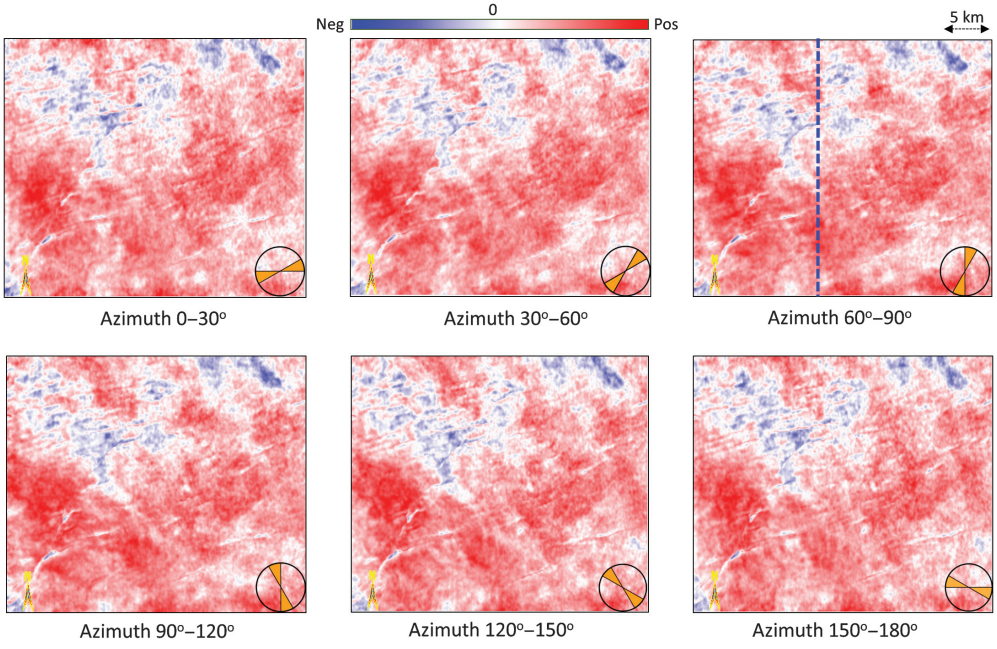

Figure 10. Stratal slices 22 ms below a horizon at approximately 1950 ms from six azimuthally limited partial stack seismic amplitude volumes. The seismic data are from the STACK trend in Oklahoma (data courtesy of TGS, Houston).

Multiazimuth coherence

A segment of an inline seismic section from the STACK trend in Oklahoma is shown in Figure 7. Inlines run north–south on the seismic survey and are indicated in Figures 8, 9, 10, and 11.

Figure 8a–8f shows six stratal slices from the azimuthally limited (30° increments) seismic data volumes. The stratal slices have been generated at a level 12 ms above a horizon at 1950 ms on the seismic data. The 288 fold wide-azimuth seismic data are from the STACK trend in Oklahoma, USA. The key steps in the processing included azimuthally compliant premigration noise attenuation, 5D interpolation to a set of regularly sampled azimuthal spokes, azimuthal velocity analysis, and spoke-by-spoke postmigration noise attenuation. Not only are there changes in the definition of the main channel running almost north–northwest to south–southeast, but there are also differences in the definition of subtle faults in the northeast–southwest direction.

Figure 9 shows the equivalent slices from the energy ratio coherence run on the azimuthally limited seismic volumes as well as the full-azimuth stack, as well as the equivalent stratal slice from the multiazimuth coherence. Notice the somewhat lower signal-to-noise ratio on the azimuthally limited coherence stratal slices compared with the full-azimuth stack. The multiazimuth coherence slice captures discontinuities that are consistent across multiple azimuthally limited volumes, weighting them by the amplitude of the data (or the strength of the illumination). Note that the channel and the east–west faults are better delineated than on the full-azimuth coherence volume. The individual azimuthally limited coherence volumes are shown for comparison, but for most practical purposes, the multiazimuthal coherence contains most of the detail in a single image.

Similarly, in Figures 10 and 11, we show a set of stratal slices from the same seismic volumes as shown in Figures 8 and 9, but at a level 22 ms lower than the horizon. Again, notice the east–west aligned fault definitions, as well as the northeast–southwest-aligned en-echelon faults on the multiazimuth coherence, which stand out from all other images.

Figure 12 shows a stratal slice 78 ms below a horizon at approximately 1700 ms from the (Figure 12a) energy ratio coherence computed on a full-azimuth seismic volume and (Figure 12b) the multiazimuth energy ratio coherence. Notice the enhanced definition of the channel features on the multiazimuth coherence as shown in the magenta and green highlighted areas. The seismic data are from the STACK trend in Oklahoma.

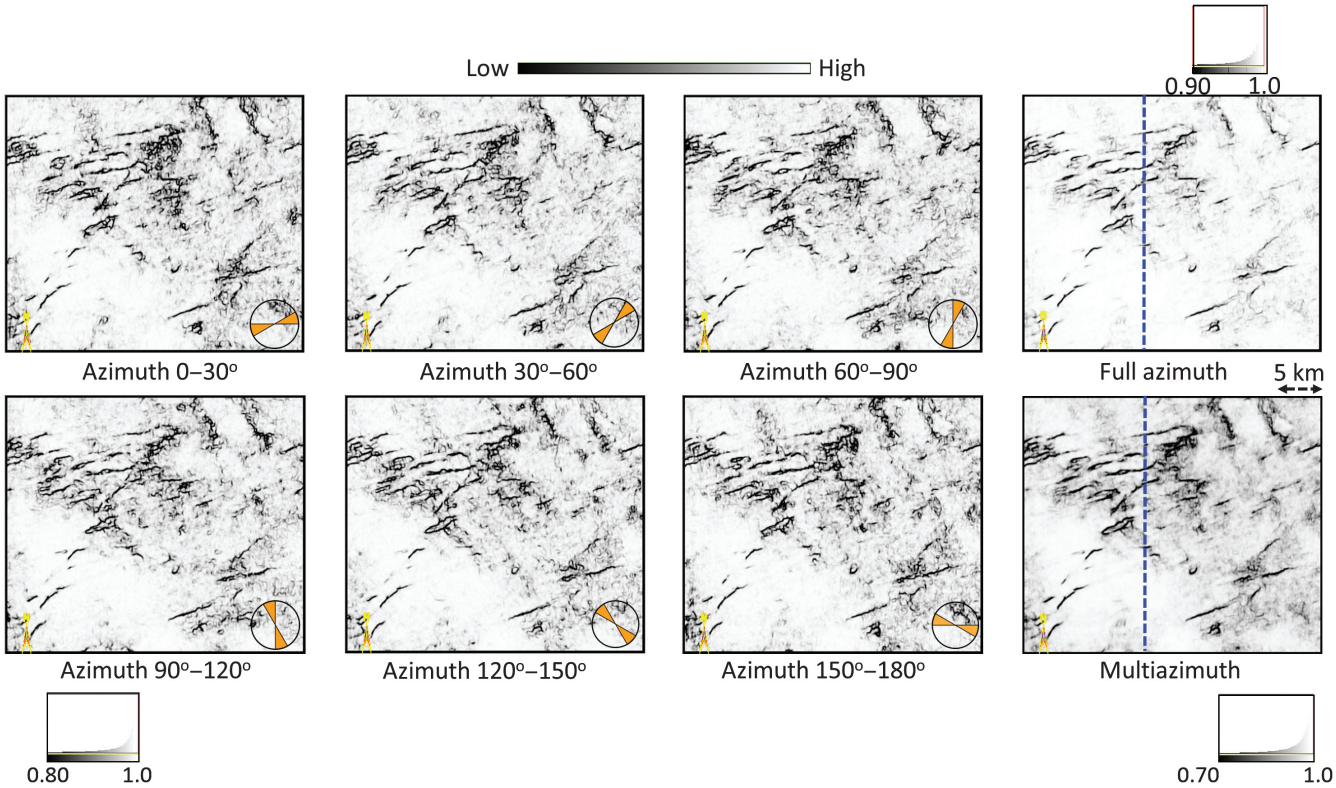

Figure 11. Stratal slices 22 ms below a horizon at approximately 1950 ms through coherence volumes computed from the six azimuthally limited partial stack amplitude volumes shown in Figure 10, from the full stack volume, and using a multiazimuth coherence algorithm. Again, the multiazimuth coherence display stands out much better than the other displays. The seismic data are from the STACK trend in Oklahoma (data courtesy of TGS, Houston).

Multioffset coherence

Multioffset coherence can be generated in the same way as multiazimuth coherence, by replacing the input azimuthally limited seismic volumes with the offset-limited seismic volumes. In general, the reflection events at larger offsets not only lose some frequency content but they also become noisier. Appropriate mute patterns are used on the gathers to capture the maximum amount of signal and to ensure the best signal-to-noise ratio. Thus, despite the best efforts at doing this, some-

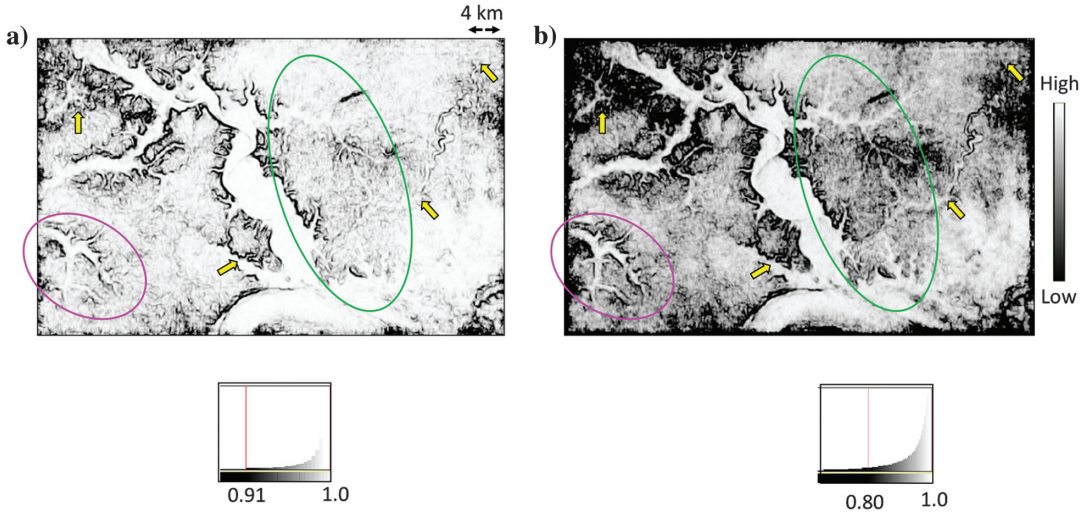

Figure 12. Stratal slice 78 ms below a horizon at approximately 1700 ms from (a) energy ratio coherence computed on the full-azimuth seismic volume and (b) the multiazimuth energy ratio coherence. Notice the enhanced definition of the channel features on the multiazimuth coherence as shown in the magenta and green highlighted areas. The seismic data are from the STACK trend in Oklahoma (data courtesy of TGS, Houston).

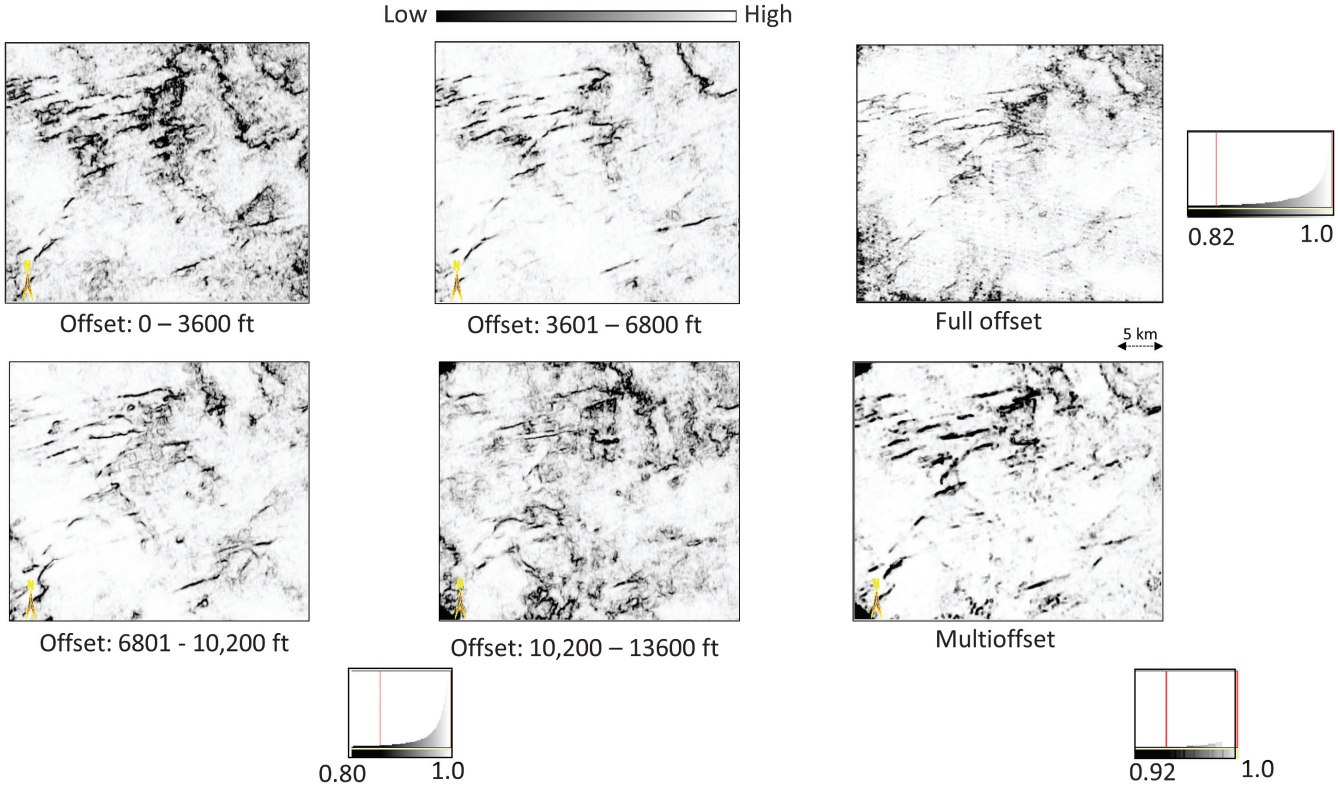

Figure 13. Stratal slices 12 ms above a horizon at approximately 1950 ms through coherence volumes computed from the four offset-limited partially stacked volumes, from the full stack volume, and using a multioffset coherence algorithm. The definition of the faults is clearer and more focused on the multioffset coherence display when compared with the other displays. The seismic data are from the STACK trend in Oklahoma (data courtesy of TGS, Houston).

times the full-offset stacked volume may not show a high signal-to-noise ratio. While generating the multioffset coherence, care can be taken to examine the offset-limited seismic volumes for their quality and then determine which ones should be used for the generation of multioffset coherence.

Figure 13 shows stratal slices 12 ms above a horizon from a data volume from the STACK trend of Oklahoma, USA. The coherence display from the full-offset coherence volume shows the lineaments as somewhat diffused, and the four individual limited-offset coherence volumes do not yield displays that can compare with the multioffset coherence volume.

Conclusion

Coherence run on spectrally decomposed seismic volumes, especially the ones at higher frequencies within the seismic bandwidth, exhibit higher lateral resolution. Instead of running the energy ratio coherence computation on many individual volumes, we make use of multispectral coherence computation by summing the covariance matrices from individual computation windows and generating the energy ratio attribute.

The coherence attribute has traditionally been run on stacked seismic data. With more powerful workstations, we can now examine coherence attribute computations on prestack data. The energy ratio coherence computation in these cases can be done by summing the covariance matrices in the computation windows from different input volumes and carried out in a single run.

The computation time for the multispectral energy ratio is approximately three times higher than the time it takes for a conventional energy ratio coherence computation for the same input parameters.

For the data sets under study, the results from their different coherence computations exhibit encouraging results.

1) Multispectral, multiazimuth, and multioffset/angle coherence computations exhibit higher signal-to-noise ratios and higher lateral resolution than conventional poststack coherence of full stack volumes.
2) Interpretations carried out on such coherence volumes will be less ambiguous.
3) Such coherence volumes can be used for extracting more information by way of fault probability volumes or tools such as ant tracking, which are likely to provide more detail for interpretation. The imaged data, however, still need to be interpreted, and such detail extracted from the input seismic data through the methods described in this paper may improve the interpretation.

Acknowledgments

We thank TGS, for the data permissions as well as the permission to present this work. The first author would like to thank R. K. Sharma, T. Strandberg, and F. Ogunsuyi for help with the processing and retrieval of the input seismic data volumes.

Data and materials availability

The real data in this paper are confidential and cannot be released.

References

Bahorich, M. S., and S. L. Farmer, 1995, 3-D seismic coherency for faults and stratigraphic features: The Leading Edge, **14**, 1053–1058, doi: 10.1190/1.1437077.

Bakker, P., 2003, Image structure analysis for seismic interpretation: Ph.D. thesis, Technische Universiteit.

Chopra, S., and K. J. Marfurt, 2007, Seismic attributes for prospect identification and reservoir characterization: SEG, Geophysical Development Series.

Chopra, S., and K. J. Marfurt, 2008, Gleaning meaningful information from seismic attributes: First Break, **26**, 43–53.

Chopra, S., and K. J. Marfurt, 2016, Spectral decomposition and spectral balancing of seismic data: The Leading Edge, **26**, 936–939.

Chopra, S., and K. J. Marfurt, 2018a, Coherence attribute applications on seismic data in various guises — Part 1: Interpretation, **6**, no. 3, T521–T529, doi: 10.1190/INT-2018-0006.1.

Chopra, S., and K. J. Marfurt, 2018b, Coherence attribute applications on seismic data in various guises — Part 2: Interpretation, **6**, no. 3, T531–T541, doi: 10.1190/INT-2018-0007.1.

Dewett, D. T., and A. A. Hensa, 2015, Spectral similarity fault enhancement: Interpretation, **4**, no. 1, SB149–SB159, doi: 10.1190/INT-2015-0114.1.

Gersztenkorn, A., and K. J. Marfurt, 1999, Eigenstructure-based coherence computations as an aid to 3D structural and stratigraphic mapping: Geophysics, **64**, 1468–1479, doi: 10.1190/1.1444651.

Grimm, R. E., H. B. Lynn, C. R. Bates, D. R. Phillips, K. M. Simon, and W. E. Beckham, 1999, Detection and analysis of naturally fractured gas reservoirs: Multiazimuth seismic surveys in the Wind River basin, Wyoming: Geophysics, **64**, 1277–1292, doi: 10.1190/1.1444634.

Henderson, J., S. Purves, G. Fisher, and C. Leppard, 2008, Delineation of geological elements from RGB color blending of seismic attribute volumes: The Leading Edge, **27**, 342–350, doi: 10.1190/1.2896625.

Libak, A., A. Behzad, and A. Torabi, 2017, Fault visualization and identification in fault seismic attribute volumes: Implications for fault geometric characterization: Interpretation, **5**, no. 2, B1–B16, doi: 10.1190/INT-2016-0152.1.

Luo, Y., S. Al-Dossary, M. Marhoon, and M. Alfaraj, 2003, Generalized Hilbert transform and its application in geophysics: The Leading Edge, **22**, 198–202, doi: 10.1190/1.1564522.

Luo, Y., W. G. Higgs, and W. S. Kowalik, 1996, Edge detection and stratigraphic analysis using 3-D seismic data: 66th Annual International Meeting, SEG, Expanded Abstracts, 324–327, doi: 10.1190/1.1826632.

Lynn, H. B., 2018a, The fabric, or internal structure, of rocks — The patterns of anisotropy. Part I: AAPG Explorer, Geophysical Corner, **39**, no. 2, 20–23.

Lynn, H. B., 2018b, The fabric, or internal structure, of rocks — The patterns of anisotropy. Part II: AAPG Explorer, Geophysical Corner, **39**, no. 3, 22–23.

Marfurt, K. J., 2017, Interpretational aspects of multispectral coherence: 79th Annual International Conference and Exhibition, EAGE, Extended Abstracts, Th A4 11, doi: 10.3997/2214-4609.201700528.

Marfurt, K. J., R. L. Kirlin, S. H. Farmer, and M. S. Bahorich, 1998, 3-D seismic attributes using a running window semblance-based algorithm: Geophysics, **63**, 1150–1165, doi: 10.1190/1.1444415.

Partyka, G. A., J. Gridley, and J. Lopez, 1999, Interpretational applications of spectral decomposition in reservoir characterization: The Leading Edge, **18**, 353–360, doi: 10.1190/1.1438295.

Pepper, R., and G. Bejarano, 2005, Advances in seismic fault interpretation automation, AAPG Search and Discovery Article 40170, http://www.searchanddiscovery.com/documents/2005/pepper/, accessed 1 November 2017.

Qi, J., F. Li, and K. J. Marfurt, 2017, Multiazimuth coherence: Geophysics, **82**, no. 6, P083–P089, doi: 10.1190/geo2017-0196.1.

Satinder Chopra received an M.Phil. (1978) in physics from Himachal Pradesh University, Shimla, India, and has 34 years of experience as a geophysicist specializing in processing, reprocessing, special processing, and interactive interpretation of seismic data. He has rich experience in processing various types of data such as vertical seismic profiling, well-log data, seismic data, as well as excellent communication skills, as evidenced by the many presentations and talks delivered and books, reports, and papers he has written. He has been the 2010–2011 CSEG Distinguished Lecturer, the 2011–2012 AAPG/SEG Distinguished Lecturer, and the 2014–2015 EAGE e-Distinguished Lecturer. He has published eight books and more than 400 papers and abstracts and likes to make presentations at any beckoning opportunity. His work and presentations have won several awards, the most notable ones being the EAGE Honorary Membership (2017), CSEG Honorary Membership (2014) and Meritorious Service (2005) Awards, 2014 APEGA Frank Spragins Award, the 2010 AAPG George Matson Award, and the 2013 AAPG Jules Braunstein Award, SEG Best Poster Awards (2007, 2014), CSEG Best Luncheon Talk Award (2007), and several others. His research interests include techniques that are aimed at the characterization of reservoirs. He is a member of SEG, CSEG, CSPG, EAGE, AAPG, and the Association of Professional Engineers and Geoscientists of Alberta.

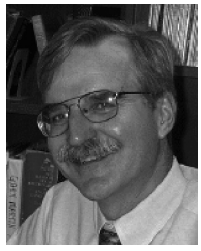

Kurt J. Marfurt received a Ph.D. (1978) in applied geophysics from Columbia University's Henry Krumb School of Mines in New York, where he also taught as an assistant professor for four years. He joined the University of Oklahoma (OU) in 2007, where he serves as the Frank and Henrietta Schultz professor of geophysics within the ConocoPhillips School of Geology and Geophysics. He worked for 18 years in a wide range of research projects at Amoco's Tulsa Research Center, after which he joined the University of Houston for eight years as a professor of geophysics and the director of the Allied Geophysics Lab. He has received the following recognitions: SEG best paper (for coherence), SEG best presentation (for seismic modeling), as a coauthor with Satinder Chopra for best SEG poster (for curvature) and best AAPG technical presentation, and as a coauthor with Roderick Perez-Altamar for best paper in *Interpretation* (on a resource play case study). He also served as the SEG/EAGE Distinguished Short Course Instructor for 2006 (on seismic attributes). In addition to teaching and research duties at OU, he leads short courses on attributes for SEG and AAPG. He currently serves as deputy editor of the SEG/AAPG publication *Interpretation*. His primary research interests include the development and calibration of new seismic attributes to aid in seismic processing, seismic interpretation, and reservoir characterization. Recent work has focused on applying coherence, spectral decomposition, structure-oriented filtering, and volumetric curvature to mapping fractures and karst with a particular focus on resource plays.